Science
AAAS

Extending Earthquakes' Reach Through Cascading
David Marsan, *et al.*
Science **319**, 1076 (2008);
DOI: 10.1126/science.1148783

Science (print ISSN 0036-8075; online ISSN 1095-9203) is published weekly, except the last week in December, by the American Association for the Advancement of Science, 1200 New York Avenue NW, Washington, DC 20005.

12. P. Stallknecht, H. Kohl, *Ultramicroscopy* **66**, 261 (1996).
13. E. C. Cosgriff, M. P. Oxley, L. J. Allen, S. J. Pennycook, *Ultramicroscopy* **102**, 317 (2005).
14. H. Kohl, H. Rose, *Adv. Imaging. Electron Phys.* **65**, 173 (1985).
15. D. A. Muller, J. Silcox, *Ultramicroscopy* **59**, 195 (1995).
16. R. F. Egerton, *Electron Energy Loss Spectroscopy in the Electron Microscope* (Plenum, New York, ed. 2, 1996).
17. P. Trebbia, N. Bonnet, *Ultramicroscopy* **34**, 165 (1990).
18. J. G. Chen, *Surf. Sci. Rep.* **30**, 1 (1997).
19. D. A. Muller, N. Nakagawa, A. Ohtomo, J. L. Grazul, H. Y. Hwang, *Nature* **430**, 657 (2004).
20. K. Dorr *et al.*, *J. Appl. Phys.* **89**, 6973 (2001).
21. X. Hong, A. Posadas, C. H. Ahn, *Appl. Phys. Lett.* **86**, 142501 (2005).
22. M. Izumi *et al.*, *Phys. Rev. B* **64**, 064429 (2001).
23. The instrument was developed under NSF grant DMR-9977547 with an additional contribution from Cornell University. In-kind contributions were made by Gatan Inc., Sandia National Laboratory, Pacific Northwest Laboratory, and Bell Laboratories. Supported by NSF Nanoscale Science and Engineering Initiative grant EEC-0117770 (D.A.M. and J.S.), NSF Materials Research Science and Engineering Center grant DMR-0520404 (L.F.K.), the TEPCO Research Foundation (H.Y.H.), and the Japan Society for the Promotion of Science (J.H.S.).

Supporting Online Material

www.sciencemag.org/cgi/content/full/319/5866/1073/DC1
Materials and Methods
Figs. S1 to S3
References

6 August 2007; accepted 18 January 2008
10.1126/science.1148820

Extending Earthquakes' Reach Through Cascading

David Marsan* and Olivier Lengliné

Earthquakes, whatever their size, can trigger other earthquakes. Mainshocks cause aftershocks to occur, which in turn activate their own local aftershock sequences, resulting in a cascade of triggering that extends the reach of the initial mainshock. A long-lasting difficulty is to determine which earthquakes are connected, either directly or indirectly. Here we show that this causal structure can be found probabilistically, with no a priori model nor parameterization. Large regional earthquakes are found to have a short direct influence in comparison to the overall aftershock sequence duration. Relative to these large mainshocks, small earthquakes collectively have a greater effect on triggering. Hence, cascade triggering is a key component in earthquake interactions.

Earthquakes of all sizes, including aftershocks, are able to trigger their own aftershocks. The cascade of earthquake triggering causes the seismicity to develop complex, scale-invariant patterns. The causality of "mainshock A triggered aftershock B," which appears so obvious if mainshock A happens to be large, must then be modified into a more subtle "mainshock A triggered C1, which triggered C2, ..., which triggered B." This has paramount consequences: The physical mechanism that causes direct triggering (static or dynamic stress changes, fluid flow, afterslip, etc.) cannot be studied by looking at aftershocks that were not directly triggered by the mainshock. Moreover, if indirect triggering is important in the overall aftershock budget (*1*–*3*), then direct triggering must be confined to spatial ranges and times shorter than the size of the total

Laboratoire de Géophysique Interne et Tectonophysique, CNRS, Université de Savoie, 73376 Le Bourget du Lac, France.

*To whom correspondence should be addressed. E-mail: david.marsan@univ-savoie.fr

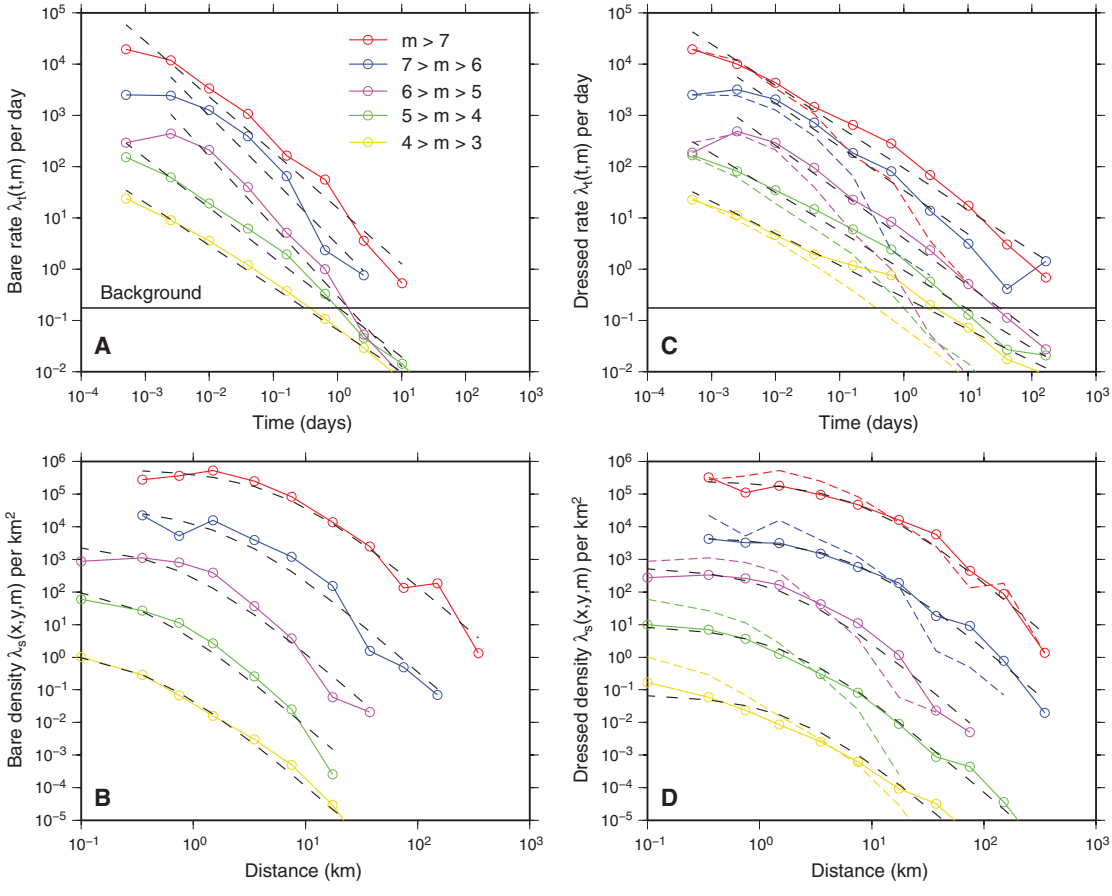

Fig. 1. Estimated rates and densities for California. (**A** and **B**) Bare kernels; (**C** and **D**) dressed kernels. The best power laws for the temporal rates $\lambda_t(t, m)$ and the best $[1 + (r/L)]^{-3}$ laws for the densities $\lambda_s(x, y, m)$ are shown as black dashed lines. The background temporal rate $\lambda_{0,t}$ [black horizontal line in (A) and (C)] is computed as $\sum_{i=1}^{N} w_{0,i}/T$. In (C) and (D), the dressed kernels (continuous lines) are compared to the bare ones (color dashed lines). The densities λ_s have been vertically shifted for clarity.

aftershock sequence. How much shorter is still an open question, in the absence of any simple or standard way to efficiently discriminate direct and indirect triggering in the data.

Seismologists mostly resort to declustering algorithms to separate earthquakes between mainshocks and aftershocks (*4*–*7*). These methods have arbitrary rules and are heavily parameter-dependent. Recently, more sophisticated methods were proposed to perform stochastic declustering—that is, determining the probability that earthquake A triggered earthquake B (*8*). This overseeds the usual approach of binary linking of one aftershock to one single mainshock: An earthquake j is then influenced by all preceding earthquakes i, according to influence weights $w_{i,j}$. These methods, however, are model-dependent, as the influence of a trigger earthquake is constrained to follow a specific law, whose parameters must be inverted.

Here we show that the probability of directly and indirectly triggering aftershocks can be estimated with no a priori model. A rapidly converging algorithm with a small number of hypotheses (linearity, mean-field) can decipher the complex seismicity time series to reveal the underlying triggering influences exerted by earthquakes of all sizes. A notable result is that even large earthquakes causally trigger aftershocks only during a relatively short time span. However, they condition regional seismicity for a much longer time period, and over larger, time-increasing distances, through the local triggering caused by their aftershocks. This cascading effect, dominated by small shocks, thus appears to be a crucial component in earthquake interactions.

Seismicity is considered as a point process in time, space, and magnitude. The observed (dressed) seismicity rate density $\lambda(x, t)$, defined as the number of earthquakes per unit time and unit area at position x and time t, is modeled as

$$\lambda(x,t) = \lambda_0 + \sum_{t_i<t} \lambda_i(x,t) \qquad (1)$$

where λ_0 is the uniform background rate density, and $\lambda_i(x, t)$ is the (bare) contribution of earthquake i that occurred at $\{x_i, t_i\}$, representing the aftershocks directly caused by this earthquake. We assume only that (i) the triggering process is linear [i.e., the bare contributions $\lambda_i(x, t)$ sum up], and (ii) a mean-field response to the occurrence of an earthquake can be estimated that depends only on its magnitude, $\lambda_i(x, t) = \lambda(|x - x_i|, t - t_i, m_i)$, hence two earthquakes of equal magnitude are modeled similarly.

The algorithm works as follows:

1. Knowing an a priori bare kernel $\lambda(|\Delta x|, \Delta t, m)$ and λ_0, we compute the triggering weights $w_{i,j} = \alpha_j \lambda(|x_j - x_i|, t_j - t_i, m_i)$ if $t_i < t_j$, $w_{i,j} = 0$ otherwise, and the background weights $w_{0,j} = \alpha_j \lambda_0$. The normalization coefficients α_j are such that

$$\sum_{i=1}^{j-1} w_{i,j} + w_{0,j} = 1 \qquad (2)$$

2. The updated bare rates are then computed as

$$\lambda(|\Delta x|, \Delta t, m) = \frac{1}{N_m \times \delta t \times S(|\Delta x|, \delta r)} \sum_{i,j \in A} w_{i,j} \qquad (3)$$

where A is the set of pairs such that $|x_i - x_j| = |\Delta x| \pm \delta r$, $m_i = m \pm \delta m$, and $t_j - t_i = t \pm \delta t$ (δr, δt, and δm are discretization parameters), N_m is the number of earthquakes such that $m_i = m \pm \delta m$, and $S(|\Delta x|, \delta r)$ is the surface covered by the disk with radii $|\Delta x| \pm \delta r$. The a posteriori background rate is

$$\lambda_0 = \frac{1}{T \times S} \sum_{j=1}^{N} w_{0,j} \qquad (4)$$

where T is the duration of the time series (containing N earthquakes) and S is the surface analyzed. This corresponds to stacking all the aftershocks following mainshocks i of similar magnitudes, but counting an aftershock j according to its weight $w_{i,j}$.

Starting with an initial guess for $\lambda(|\Delta x|, \Delta t, m)$, these two steps are iterated until

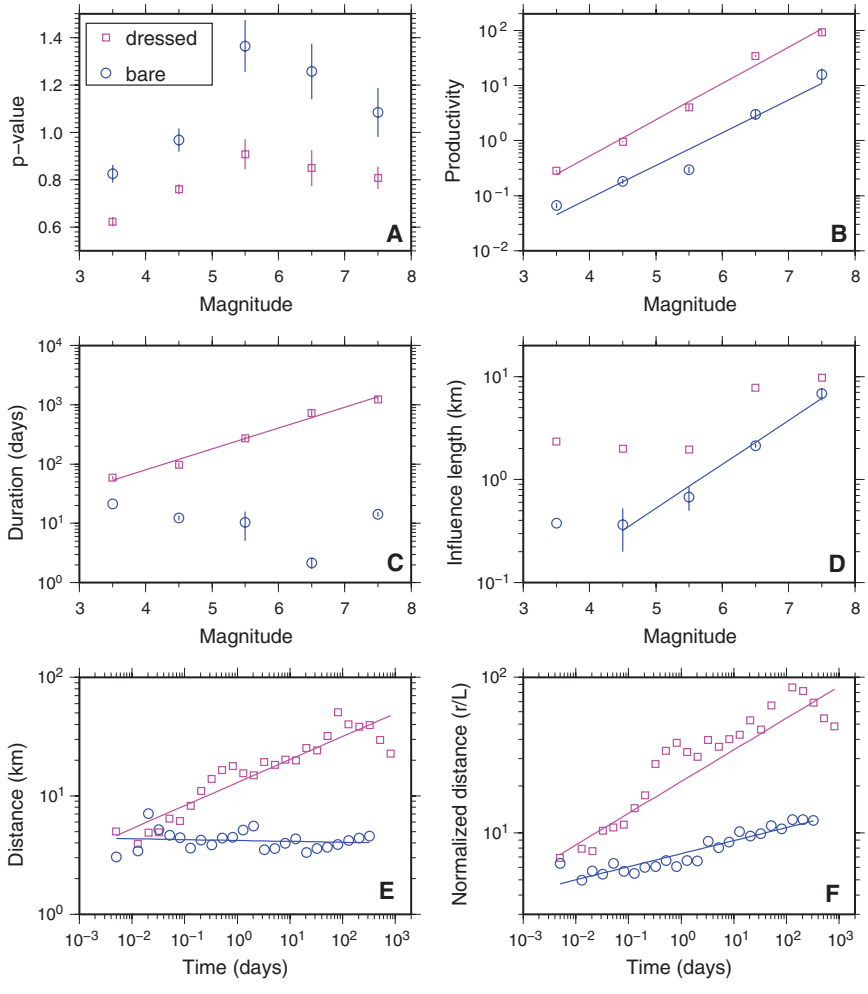

Fig. 2. Characteristics of bare (blue) and dressed (purple) aftershock sequences. (**A** and **B**) p values and productivity parameters χ from the fits $\lambda_t(t, m) = \chi t^{-p}$ of Fig. 1. Productivity grows as $10^{0.60\pm0.07m}$ (bare) and $10^{0.66\pm0.04m}$ (dressed). (**C**) Durations of the sequences. The dressed duration follows $10^{0.35m}$. (**D**) Influence lengths L estimated from the $[1 + (r/L)]^{-3}$ fits of the spatial densities. (**E**) Mean epicentral distance between mainshocks and aftershocks versus time following the mainshock. (**F**) Same as (E), for epicentral distance normalized by the bare influence length L of the mainshock. The best power laws $r \sim \delta t^H$ give (E) $H = -0.01 \pm 0.03$ (bare), H = 0.19 ± 0.04 (dressed), and (F) $H = 0.08 \pm 0.02$ (bare), H = 0.21 ± 0.06 (dressed).

convergence is reached—that is, until the weights (or the rates) do not change substantially during an iteration. Tests were conducted on synthetic catalogs, showing the ability of the algorithm to correctly estimate the cascade structure (*9*).

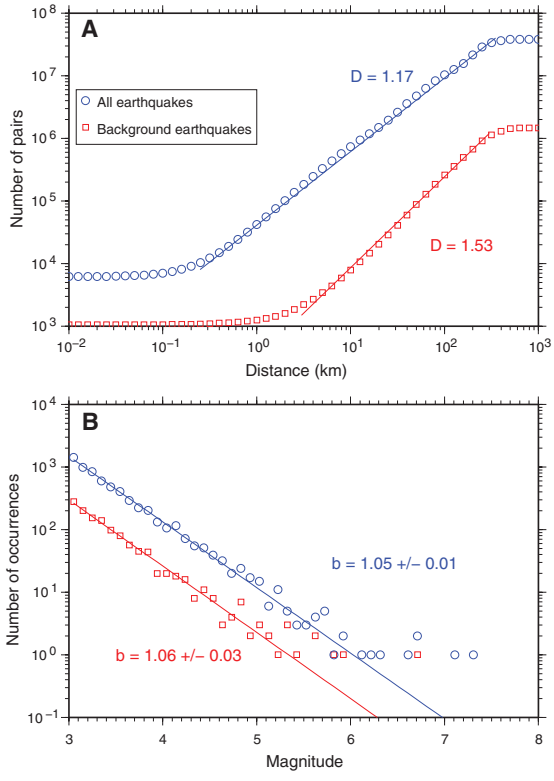

Fig. 3. Comparison of total (blue) and background (red) seismicity. (**A**) Number of pairs $N(r)$ with epicentral distance less than distance r, along with estimates of the fractal correlation dimension D such that $N(r) \sim r^D$. (**B**) Number of occurrences versus magnitude, scaling as $10^{-b \times m}$.

We analyzed seismicity in southern California (*10*) from 1 January 1984 to 31 December 2002. We considered only the $N = 6190$ $m \geq 3$ earthquakes in the catalog, both for completeness reasons and because the method uses a $N \times N$ weight matrix, preventing the analysis of too large a data set on a standard desktop computer. The completeness magnitude is estimated to be 2.2 for this catalog. The method was slightly modified to account for the fact that the background earthquakes are nonuniformly distributed in space (*9*).

The rates had roughly an Omori-Utsu decay $\lambda_t(t, m) = \chi t^{-p}$ (Fig. 1), where χ is the productivity. The p value increased with m (Fig. 2A), as observed previously (*11*) for dressed aftershock sequences, although with a saturation at $m \geq 6$. The rates decayed significantly more slowly when considering the full cascade including indirectly triggered aftershocks. The dressed p values were 0.2 to 0.4 units smaller than the bare p values (Fig. 2A). The productivity parameter grew as $= \chi \sim 10^{am}$, with $a = 0.60 \pm 0.07$ and $a = 0.66 \pm 0.04$ for the bare and dressed kernels, respectively (Fig. 2B). This yielded a significantly lower scaling exponent than previous estimates (*3*, *12*–*14*) for dressed sequences.

The densities were well fitted with a $\lambda_s(x, y, m) \sim [1 + (r/L)]^{-3}$ law, hence a r^{-2} decay of the number of aftershocks (Fig. 1). The bare

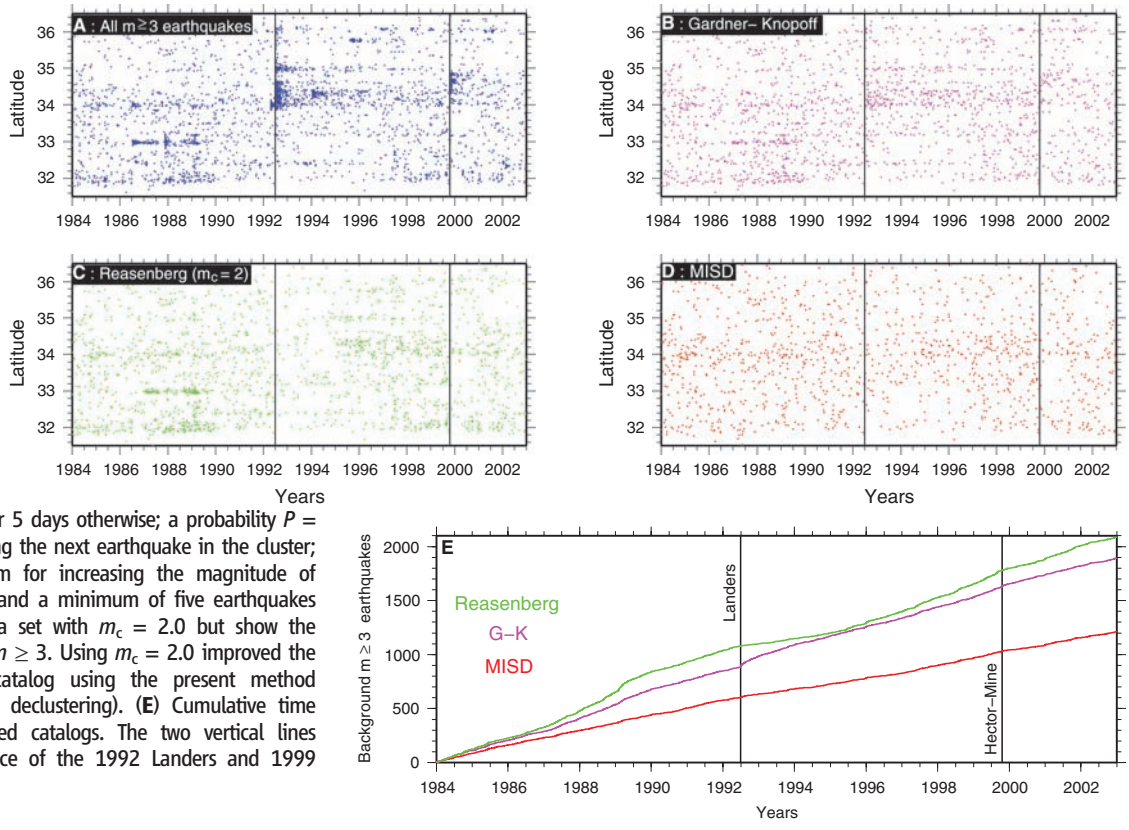

Fig. 4. Comparison of declustering algorithms. (**A** to **D**) Latitude versus time of occurrence of $m \geq 3$ earthquakes. (A) All earthquakes in the catalog. (B) Declustered catalog using the method of (*4*). (C) Declustered catalog using the algorithm of (*5*). Parameters are $r_{fact} = 8$, which gives the number of mainshock rupture lengths up to which a mainshock is supposed to trigger aftershocks; the maximum ahead-time for linking an aftershock to a cluster, which is 1 day if only one event belongs to the cluster, or 5 days otherwise; a probability $P = 95\%$ of confidence of observing the next earthquake in the cluster; $\chi_k = 0.5$, the correction term for increasing the magnitude of completeness during clusters; and a minimum of five earthquakes per cluster. We used the data set with $m_c = 2.0$ but show the declustered earthquakes with $m \geq 3$. Using $m_c = 2.0$ improved the algorithm. (D) Declustered catalog using the present method (model-independent stochastic declustering). (**E**) Cumulative time series of the three declustered catalogs. The two vertical lines indicate the time of occurrence of the 1992 Landers and 1999 Hector Mine earthquakes.

influence length L was remarkably small, ranging from 0.35 km at $4 \leq m < 5$ to 6.6 km at $m \geq 7$. It grew as $10^{0.43m}$ (Fig. 2D), which is close to the $10^{0.5m}$ dependence expected for the rupture length of small to intermediate-size earthquakes (*15*). The bare length was 0.35 km for $3 \leq m < 5$, which is due to the limited resolution on the relative hypocenter positions, as confirmed by the break in scaling at ~400 m for the correlation integral (Fig. 3A). The dressed influence lengths were about 5 times the bare ones. These influence lengths were not maximum triggering distances: Many aftershocks were triggered past L. Relaxing the point-like earthquake hypothesis affected these results for the large mainshocks. Using distances to the rupture plane rather than epicentral distances, the bare kernel of $m \geq 6$ mainshocks was moved toward longer-range triggering, greater aftershock productivity, and longer durations (*9*).

The durations of aftershock sequences (Fig. 2C) were computed by (i) calculating, for all the mainshocks, the delays after which the last direct and last indirect aftershocks occurred, and (ii) averaging these delays conditioned on the magnitude of the mainshock. The duration of direct aftershock sequence was largely independent of the mainshock magnitude and was generally short (on the order of 10 to 15 days for $m \geq 3$ aftershocks). The dressed sequence, however, lasted longer for larger mainshocks, following a $10^{0.35m}$ increase. This implies that short-lasting triggering mechanisms, acting at the time scale of a few days, could be the key process, along with the cascading effect, in controlling earthquake dynamics.

The slow expansion of aftershock zones has been reported in previous studies (*16*, *17*). We measured the mean distance r between mainshock and aftershock with time δt separating the two earthquakes. This distance was constant for bare aftershocks, whereas for dressed aftershocks it slowly grew as $r \sim \delta t^{0.19}$ (Fig. 2E). We reached similar conclusions when considering the distance normalized by the bare influence length L of the mainshock (Fig. 2F). This shows that cascading triggering drives the expansion of aftershock zones: The spatial pattern of direct triggering was almost constant with time, ruling out triggering by fluid movements or viscoelasticity at the time scales examined here.

The number of earthquakes directly triggered by all the earthquakes of a given magnitude slowly decreased with this magnitude, demonstrating the importance of small shocks in controlling the regional seismicity. The collective production scales as $10^{(a-b)m}$; here, $a = 0.6$ for the bare aftershocks (Fig. 2B) and $b = 1.05$ (Fig. 3B).

The background spatial function $g(r)$ decayed as $r^{-0.43}$, which is equivalent to saying that the background earthquake epicenters are fractally distributed with dimension $D = 1.57$. This is confirmed by the correlation integral of the background earthquakes (Fig. 3A), counting the number of pairs of earthquakes with distance less than a given value, each pair (i, j) being weighted by $w_{0,i} \times w_{0,j}$. The similar b values of the Gutenberg-Richter laws (*18*) for the total and the background earthquakes (Fig. 3B) suggest that the dynamic rupture extent is not a priori controlled by the triggering mechanism (either previous earthquakes or aseismic processes such as tectonic loading) at work.

We obtained a background rate of 0.17 $m \geq 3$ earthquakes per day in southern California over the years 1984 to 2002, which corresponds to 19.5% of the total rate of $m \geq 3$ earthquakes. The remaining ~80% can therefore be considered as resulting from stress transfer and fault interaction processes, causing the seismicity to be heavily clustered in time. Such a proportion at the magnitude cutoff $m_c = 3$ is coherent with the estimates in the range 18% to 24% we obtained using other nonparametric methods (*19*). The values computed using the present method, however, depend on m_c: Cutting at larger magnitudes increases the relative proportion of background earthquakes to 32% at $m_c = 4$ and 68% at $m_c = 5$. A larger cutoff causes the removal of small triggering earthquakes; earthquakes that were triggered by small shocks are then more likely to be seen as background earthquakes (*20*). Inversely, decreasing m_c would yield smaller percentages of background events. The 19.5% proportion at $m_c = 3$ is therefore an overestimation of the actual background contribution.

Declustering of earthquake catalogs aims at removing the aftershock clusters, keeping only statistically independent mainshocks. The declustering algorithms by Gardner and Knopoff (*4*) and Reasenberg (*5*) are the most classical methods. We ran these two methods along with ours (Fig. 4). The present method is better at identifying an underlying Poisson process, and it efficiently removes the aftershock clusters following large mainshocks such as the 1992 Landers and 1999 Hector Mine earthquakes. Moreover, it does not rely on any parameterization.

Cascading of aftershock triggering is an essential component of seismicity. It has a scale-invariant structure, making earthquake declustering an ill-defined problem: The statistical dependence between earthquakes increases when decreasing the value of m_c, so that the remaining set of declustered mainshocks heavily depends on m_c. Because of this cascading, the aftershock sequence initiated by a mainshock is substantially extended, mostly in time. Conversely, what appears at first as an aftershock cluster related to a well-identified mainshock is in fact mostly caused not by the mainshock itself, but rather by intermediate aftershocks. When decreasing m_c, the direct triggering effect due to large mainshocks could potentially be even further reduced relative to direct triggering by small shocks. This is particularly critical for understanding the physical mechanisms that cause earthquake triggering: The testing and validation of models first require the correct relation of the aftershocks to their trigger, rather than to an older, generally bigger, ancestor in the triggering chain.

References and Notes

1. K. R. Felzer, T. W. Becker, R. E. Abercrombie, G. Ekström, J. R. Rice, *J. Geophys. Res.* **107**, 2190 (2002).
2. D. Marsan, *Geophys. J. Int.* **163**, 141 (2005).
3. A. Helmstetter, Y. Y. Kagan, D. D. Jackson, *J. Geophys. Res.* **110**, B05S08 (2005).
4. J. K. Gardner, L. Knopoff, *Bull. Seismol. Soc. Am.* **64**, 1363 (1974).
5. P. Reasenberg, *J. Geophys. Res.* **90**, 5479 (1985).
6. S. D. Davis, C. Frohlich, *Geophys. J. Int.* **104**, 289 (1991).
7. G. M. Molchan, O. E. Dmitrieva, *Geophys. J. Int.* **109**, 501 (1992).
8. J. Zhuang, Y. Ogata, D. Vere-Jones, *J. Am. Stat. Assoc.* **97**, 369 (2002).
9. See supporting material on *Science* Online.
10. P. Shearer, E. Hauksson, G. Lin, *Bull. Seismol. Soc. Am.* **95**, 904 (2005).
11. G. Ouillon, D. Sornette, *J. Geophys. Res.* **110**, B04306 (2005).
12. B. E. Shaw, *Geophys. Res. Lett.* **20**, 907 (1993).
13. A. Helmstetter, *Phys. Rev. Lett.* **91**, 058501 (2003).
14. K. R. Felzer, R. E. Abercrombie, G. Ekström, *Bull. Seismol. Soc. Am.* **94**, 88 (2004).
15. C. H. Scholz, *The Mechanics of Earthquakes and Faulting* (Cambridge Univ. Press, Cambridge, 1991).
16. F. Tajima, H. Kanamori, *Phys. Earth Planet Inter.* **40**, 77 (1985).
17. A. Helmstetter, G. Ouillon, D. Sornette, *J. Geophys. Res.* **108**, 2483 (2003).
18. B. Gutenberg, C. F. Richter, *Bull. Seismol. Soc. Am.* **142**, 185 (1944).
19. S. Hainzl, F. Scherbaum, C. Beauval, *Bull. Seismol. Soc. Am.* **96**, 313 (2006).
20. D. Sornette, M. J. Werner, *J. Geophys. Res.* **110**, B09303 (2005).

21. We thank G. Daniel, A. Helmstetter, G. Ouillon, and D. Sornette for constructive discussions. Supported by European Community project VOLUME (FP6-2004-Global-3) (O.L.).

Supporting Online Material

www.sciencemag.org/cgi/content/full/319/5866/1076/DC1
Materials and Methods
SOM Text
Figs. S1 to S6
Table S1
References

3 August 2007; accepted 10 January 2008
10.1126/science.1148783